Original Article

Synthesis, Crystal Structure, Hirshfeld Surface, DFT and Molecular docking studies of (E)-3-(4-chlorophenyl)-1-(2,4-difluorophenyl)prop-2-en-1-one

T. K. Madhura[1], B. M. Rajesh[2*], K. Chandra Kumar[3], Chandra[4], Srikantamurthy N[5]

[1] Department of Education, Mount Carmel College, Bengaluru-560052, Karnataka, India.
[2] Department of Physics, R V College of Engineering, Bengaluru-560059, Karnataka, India.
[3] Department of Physics, HKBK College of Engineering, Bengaluru-560045, Karnataka, India.
[4] Department of Physics, The National Institute of Engineering (NIE),Mysore-570008, Karnataka, India.
[5] Department of Chemistry, Vidyavardhaka College of Engineering, Visvesvaraya Technological University, Mysore-570002, Karnataka, India.
Email: rajeshbm@rvce.edu.in[2]

DOI: 10.47750/pnr.2022.13.S07.359

Abstract

The Chalcone derivative (*E*)-3-(4-chlorophenyl)-1-(2,4-difluorophenyl)prop-2-en-1-one ($C_{15}H_9ClF_2O$) has been newly synthesised by one-pot Claisen-Schmidt condensation reaction. The crystal structure and the lattice parameters were obtained by a single-crystal X-ray diffraction method. A quantitative analysis of the nature of intermolecular interactions, dominant interactions and corresponding energy involved in molecular packing was carried out using Hirshfeld surface analysis. From this analysis H…H interactions showed major contributions with 24.5% and H…F showed a significant contribution with 17.7% towards overall crystal packing. The quantum mechanical calculations were performed using Gaussian software. The title compound was optimized using Density Function Theory with B3LYP hybrid functional with 6-31G(d,p) basis set. In this, the frequency, molecular orbital analysis was performed and electrostatic potential map was generated and analyzed. Further, The synthesized molecule was docked with a protein target using Autodock 4 to find the best conformation site in the target.

Keywords: Chalcone, Single crystal XRD, Hirshfeld, DFT, Molecular Docking

Graphical Abstract

The molecular structure determination using XRD, the findings of intermolecular interaction within the structure usingHirshfeld surface analysisand molecular docking studies of the synthesized molecule is discussed in this research work.

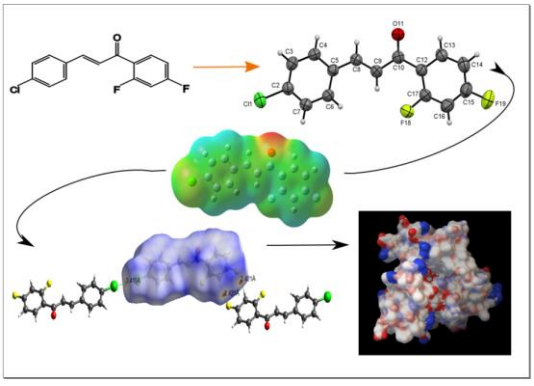

Introduction

Chalcones are one of the simple chemical scaffolds which are found in many naturally occurring organic compounds [1]. These belong to the flavonoid family found in fruits and vegetables [2]. The structure of Chalcone is as shown in Figure 1.The literature survey on Chalcones and its derivatives showcases a broad spectrum of its clinical potentials and biological activities. They show a pivotal role in medicinal chemistry, and biological and pharmacological activities[3]. This scaffold has demonstrated potential forthe prevention and treatment of cancer. They are found to play a pivotal role in commercial applications like antibacterial, antifungal, antiviral, anti-inflammatory, hepatoprotective and anti-ulcerative activities.Further, the crystal structure of the titled compound was studied experimentally and theoretically using XRD and DFT respectively. Intermolecular interactions were studied using Hirshfeld surface analysis. Theoretical predictions of the molecular docking studies were done with the Auto Dock tool. In the present study, to validate the experimental crystallographic data for the title compound with the results of theoretically optimized structure calculations based on available basis set methods. Subsequently, correlated optimized structure with the experimental data shows good agreement [4, 5]. Frontier molecular orbital (FMO) analysis were done to obtain the information like quantum physical parameters, chemical softness/hardness, chemical potential and electrophilicity/electronegativity[6, 7].

Experimental detail

SYNTHESIS

Synthesis of chalcone: (E)-3-(4-chlorophenyl)-1-(2,4-difluorophenyl)prop-2-en-1-one (3):The synthesis of chalcone (3)was carried out by utilizing a reported method with slight modifications as shown in scheme 1[8].The reaction was carried out by adding 5 mmol of 1-(2,4-difluorophenyl)ethanone(1)into 5 mL of ethanol in a round bottom flask, then 5 mmol of 4-chlorobenzaldehyde (2)was added to the flask. Then, to the mixture was added 10 mL of 60% KOH solution slowly with continuous stirring for 1.5 hours. After the KOH addition, the mixture wasstirredagain for 14 to 16 hours at room temperature. After the completion of the reaction tested by TLC, the reaction mixture was added with 10% HCl of 1.5 mL. Then the crude product formed was filtered with a Buchner filter until the precipitate is separated from the filtrate. Then the crude solid waswashed with cold waterand dried at room temperature. Furthermore, recrystallization was done with cold ethanol and adopted a slow evaporation method to get a single crystal suitable for X-ray diffraction.In this reaction, enolate anions (carbanions) formed from acetophenone derivatives by hydroxide base attracting α-hydrogen.β-hydroxy carbonyl intermediates formed from carbanion by attracting carbonyl of benzaldehyde derivatives. This produced Chalcone under the acidic condition [9].

Scheme 1: Synthesis of (E)-3-(4-chlorophenyl)-1-(2,4-difluorophenyl)prop-2-en-1-one

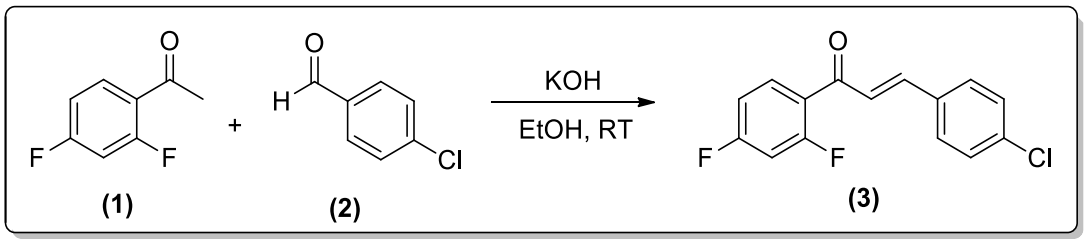

SINGLE-CRYSTAL X-RAY DIFFRACTION

The molecular structure of the titled compound is studied using the single-crystal X-ray diffraction method by Bruker SMART APEX II diffractometer with a detector area of resolution 18.4 units. The graphite-monochromated MoKα X-ray source was used for diffraction with a wavelength of 0.71073 Å at 293 K. Totally, 9284 reflections were measured out of which 2755 reflections were found to be unique and 1616 reflections were intense. The structure determination and refinement are done for 2755 reflections and 172 crystal parameters are refined [10].

The XRD data is retrieved in hkl format and used for further computational methods. The obtained raw data were reduced using SHELXS and solved using by SHELXL[11, 12]. The structure refinement was performed by full-matrix least-squares methods on F^2 by usingsoftware package and computed using PLATON [13, 14]. Refinement was carried out by the removal of unwanted atoms from the molecule. The refinement of non-hydrogen atoms was done with anisotropic displacement coefficients. All hydrogen atoms were placed geometrically and allotted isotropic displacement coefficients with a riding model to refine the small molecule X-ray data. The refined data (R=0.0529) is obtained in Crystallographic file format (.cif) and used for further calculations. The ORTEP diagram of the molecule was generated using MERCURY software.Crystallographic dataof newly synthesized $C_{15}H_9ClF_2O$compound has been deposited at the Cambridge Crystallographic Data Center (CCDC deposit no.2151070).

COMPUTATIONAL METHODS:

Computational studies of the title compound are performed using Crystal Explorer 17, Gaussian 16 and Autodock 4.0. Hirshfeld surfaces were named after FL Hirshfeld. He elaborates a meaningful definition of molecule in a crystal. The Hirshfeld surface defines the space filled by a molecule in a crystal by partitioning the crystal electron density into molecular fragments. It is a novel way of defining packing modes and intermolecular interactions in molecular crystals through visualization and using fingerprint plotsfor quantitative analysis of intermolecular interactions. The title compound was optimized using Density Function Theory with B3LYP hybrid functional with 6-311G(d,p) basis set. Using FMO analysis, HOMO-LUMO energies are computed. Vibrational spectra such as IR and UV Visible spectra are studied. A molecular electrostatic potential map was generated and analyzed. To understand the binding modes of the synthesized titled compound, a molecular docking study was carried out with 1KZN protein. It is to find the best fit conformation of a ligand with protein 1KZN [15–17].

Results and discussions

X-RAY DIFFRACTION STUDIES

The detailed crystal structure of the (*E*)-3-(4-chlorophenyl)-1-(2,4-difluorophenyl)prop-2-en-1-one was obtained using a single crystal X-ray diffraction method. The results shows that synthesized crystal is formed in a triclinic lattice with *p-1* space group. The values of cell edges are found as a= 3.961 Å, b=6.010 Å and c=26.069 Å. The Interfacial angles α=92.452°, β= 91.025° and γ=92.483° confirm the triclinic formation of the unit cell. The unit cell parameters obtained from the cif file are listed in Table 1. Bond length and bond angles of the experimental data of the titled compound is tabulated in Table 9 and 10 respectively. The ORTEP diagram of the molecule drawn with the 50% thermal ellipsoids is shown in Figure 2. The packing diagram of crystallographic unit cell of the molecule is shown in Figure 3.

HIRSHFELD SURFACE ANALYSIS

The nature of intermolecular interactions and their contributions to the supramolecular assembly was quantified and carried out using Hirshfeld studies. The HS shows the entire molecule in the crystal into regions of different colors representing varying molecular electron density distribution. These colored interpretations are very useful

to analyze the weak intermolecular interactions significantly [18]. The crystallographic information file of the title molecule was used as an input file and the HS associated with 2 dimensional fingerprint plots were generated using softwareCrystal Explorer 17.

The red shade of HS on d_{norm} is coded for shorter interatomic contacts having contact length less than Van der Waal separation and the blue shade indicates d_{norm} is coded for contact distance greater than Van der Waal separation [19]. The white shade of the map represents the contact distance equivalent to Van der Waal's radii as shown in Figure 4 [20]. In the titled molecule, three red spots were observed in d_{norm}. H…F reciprocal atoms with bond length 2.421 Å and Cl…Cl reciprocal atoms with a bond length 3.411 Å were located within the radius of 3.80 Å from the reference atom and are shown in Figure 5. It is found that d_{norm}= -0.0962 Å to 1.2470 Å with the mean of 0.4313 Å, d_i = 1.082 Å to 2.4418 Å with the mean of 1.7503 Å and d_i =1.0829 Å to 2.5357 Å with the mean 1.7596 Å. The HS has found to have an area of 291.65 $Å^2$.Volume, globularity and asphericity of the HS of the titled compound are 303.54 $Å^3$, 0.749 and 0.429 respectively and tabulated in Table 2.

The shape index gives the measurement of the shape of HS quantitatively and shows local shape geometry. It shows HS having a complimentary map with bumps and hollows. The blue bump belongs to donor electro molecular interactions having index >1 and the red hallow belongs to the accepter of electro molecular interactions having index <1 [21]. From HS studies it is found that Shape index = -0.9925 au to 0.9989 au having a mean value of 0.2757 au. The red and blue adjacent triangles visible in the shape index shown in Figure 6(a,b) reveal the possibility of π-π stacking interactions between the molecules. The blue triangle is a flat region formed at the adjacent carbon ring of the molecule inside the surface and the red triangle is a concave region formed by the carbon atoms of π stacked molecule above it. The root-mean-square curvature of the surfacein the crystal structure was displayed by a function called curvedness which shows relatively flat green region separated by a blue edge[22, 23].The HS mapped on curvedness on the entire space having flat green irregular region surrounded by sharp blue edges asshown in Figure 7. This helps to analyze contact faces between the surfaces and also to locate the regions of π-π stacking interactions adjacent to blue edges. These π-π interactions are visible as flat green regions adjacent to edges on the surface where the dark blue edge regions can be assumed as the absence of π-π interactions [24]. It is found that Curvdness = -4.0 au to 4.0 au having the mean value of -1.0717 au. HS mapping with fragment patch varies from 0to 13 with the mean value of 6.92 will show the electron density of the entire crystal is divided into a molecular fragment and shown in Figure 8.

FINGERPRINT PLOT:

The crystal explorer computation provides high-resolution 2D fingerprint plots representing the complex information about the crystal packing and gives the visual symmetry of the intermolecular interactions [25]. It plots different interactions throughout the crystal packing. These visual graphical plots can be generated by enclosing all intermolecular contacts which can be expected in the crystal. The d_{norm} and 2D fingerprint plots were used to decode the intermolecular interactions in the crystal lattice and the results are quantified and tabulated. Fingerprint plots were generated using the translated 0.5 Å range with very high resolution and includs reciprocal contacts.For the titled compound, the interatomic interactions contributing maximum toa minimum towards overall crystal packing are quantified and shown. 2D fingerprint plot of H…H interactions shows a diffused needle-shaped surface and emerges as a major contribution with 24.5%. The 2D plot of F…H interactions shows a pair of sharp spikes with a 17.7% of significant contribution towards overall crystal packing [26]. The interactions with their percentage of interaction are shown in Table 3.

INTERNAL ENERGY CALCULATIONS:

The crystal exploration allows us to evaluate interaction energies within the multi-component crystal. The software provides two energy models, one for faster calculations and the otherto increase the accuracy of the calculations and they are CE-HF ... HF/3-21G electron densities and CE-B3LYP ... B3LYP/6-31G(d,p) electron densities respectively [27]. These calculations provide pair-wise interaction energies and displays in different color codes. The total energy calculated by these programs has four energy components and they are electrostatic,

polarization, dispersion and exchange repulsion energy components. The title molecule is selected, and a cluster molecule within the radius is formed and subjected to the energy calculations. The scale factors are tabulated in Table 4.

ENERGY FRAMEWORKS

The building of energy frameworks gives the 3D picturisation of the supramolecular clustergenerated around 3.8 Å of the molecules in a crystal. The four components of the energy of molecular interaction are electrostatic (E_ele = 1.057), polarization (E_pol= 0.740), dispersion (E_dis= 0.871), and exchange-repulsion (E_rep= 0.618)[27]. The molecular pair-wise interaction energies are listed in the Table 5 shows that the dispersion energy is morethan electrostatic energy. Figure 10 shows the molecular pairs along *a* axis is involved in the calculation of interaction energies. The size of the cylinders in the energy frameworks describes the strength of the interaction energy and also the molecular packing.

MOLECULAR DOCKING STUDIES

Docking studies for the title compound were performed using Autodock-4.2 with the Lamarckian Genetic Algorithm (LGA) computational method. The binding affinity and the interaction between enzymes and ligand of the title molecule were studied and summarised in Table 6[28].

For the docking, a 3D protein structure was retraived from RSCB (PDB Code: 1KZN). Several binding modes at various poses of the synthesized molecule docked into cancerresistant protein for the prediction of predominant binding mode. It was found that the molecule has Van der Waal interaction with the surrounding active site amino acid residue Gly77 with the interaction length of 1.88 Å isas shown in Figure 11. The docking studies showed the title molecule as a good inhibitor with inhibition constant (vdW+Hbond+desolv energy)=7.47against the protein target (1KZN). The protein-ligand complex structure in 3D provides the details of the binding mechanism between ligand and protein at the atomic level and it is shown in figure 12[29]. The minimum binding energy of the title molecule with the protein target (1KZN) was estimated as -6.99 kJ/mol and hence may be considered a good inhibitor of cancer cells[30]. The docked scores are given in Table 6. The ligand and receptor complex is shown in Figure 12.The 3D structure of the protein-ligand complex givesdetailedinformation of the binding mechanism between ligand and target protein at the atomic level.

DENSITY FUNCTIONAL THEORY

Themolecular structure of the newly synthesized chalcone derivativeshown in Figure 13 was fully optimized using the density functional theory with B3LYP (Becke three-parameter Lee–Yang–Parr) hybrid functional groups 6-31G(d,p) basis set in ethanol solvent. The optimized structure provides the bond length and bond angles of the molecule [31]. The frontier molecular orbitals, such as highest occupied molecular orbitals and lowest unoccupied molecular orbitals are crucial in understanding the electronic transmissions and charge transfer properties of the molecule [32].

The vibrational properties ofthe optimized molecule were studiedunder UV visible andIRSpectroscopic computational calculations and these graphs are shown in Figures 14(a) and 15 respectively. The absence of imaginary frequenciesis evident of the structure as true energy minima. Majority of the absorption spectroscopy of organic compounds are due to the transitions from n toπ^*or π to π^*electrons to the excited state which comes in the range of 200 to 700 nm[33]. The UV absorption spectral response shows three prominent singlet peaks at the wavelengths 396.74 nm, 339.4 nm and 305.94 nm respectively. These peaks are due to the excitation of electrons from HOMO to LUMO having energy gaps of 3.1251 eV, 3.6396 eV and 4.0525 eV respectively[34]. λ_{max} cooresponds to 339.4 nm can be assigned to $n \rightarrow \pi^*$transition and may be assigned to the excitation in the aromatic ring and C = Ogroup. $\lambda_{edge}$was found to be 405 nm and the calculated energy gap was 3.1 eV.The energy gap of

3.2 eV was found from the indirect band gap which calculated from the tauc's plot as shown in Figure 14(b)[35].The details of electronic excitations and spectral assignments are shown in Table 7.

The IR spectra obtained from the DFT calculations shown in Figure 15 reveals that, assymetric (3198,3208,3224,3225 cm^{-1}) and symmetric (3174,3227,3235,3243,3258cm^{-1}) stretching vibrations of the aromatic C-H bands are seen with low intensity bands.Ketone group that is in conjugation showed a peak at 1723 cm^{-1}. It has C=O stretching, C=C stretching, C-H assymetric and symmetric bending vibtrations. Major peaks were observed at 1626cm^{-1}(C=O stretching), 1635cm^{-1}(assymetic C-H bending), 1648cm^{-1}(assymetric C=O stretching)and 1658 cm^{-1}(C=C assyemteric and assyemetric bending) vibtrations[36].

ELECTROSTATIC POTENTIAL MAP

The molecular electrostatic potential (MEP) map was generated to get an insight into the relationship between structure and property and helps to understand the reactivity of the compounds[37]. The MEP of the title molecule is as shown in figure 16. It gives an impression ofthe total electrostatic effects produced by the net charge distribution of the molecule. This analysis helps to identify the reactive sites based on their electrostatic potential values. Here the negative regions of the electrophiles are red in color and the positive side of nucleophiles is blue in colour. The electron density of the compound is from -4.488e^{-2} to 4.488e^{-2}. The MEP map shows the red coloured negative potential regions are concentrated over the oxygen (O) atom, while the blue coloured positive potential regions spread around hydrogen atoms. The C = O group indicates the significant electrophilic attack position.

FRONTIER MOLECULAR ORBITALS

The HOMO and LUMO are generated with DFT calculations and it is shown in Figure 17. From these energies, the reactivity descriptors, such as ionization potential, electron affinity, chemical potential (μ), hardness (η), softness (S), electronegativity (χ), and electrophilicity index (ω) have been calculated and tabulated in Table 8.

Conclusions

The compound $C_{15}H_9ClF_2O$is synthesized by the Claisen-Schmidt condensation reaction.Compound was crystallized in the triclinic crystal system withP-1space group. The Hirshfeld surface analysis showed shorter interactions in the crystal between H…F atoms and Cl…Clatoms. Thedominant contribution from H…H (24.5%)and F…H (17.7%) of interactionstowards crystal packing are visualized from the fingerprint plots.The buildingof 3D energy frameworks revealed that the electrostatic energy is more over the remaining energies.The larger energy gap of 4.0 eV predicts the stability of the molecule. The red coloured negative potential regions concentrated over the oxygen (O) atomin the MEP map shows the chemical reactivity sites of the molecule. The minimum binding energy of the title molecule with the protein target (PDB Code: 1KZN) was estimated as -6.99 kJ/mol and hence may be considered a good inhibitor of cancer cells.

References

1. Ouyang, Y., Li, J., Chen, X., Fu, X., Sun, S., Wu, Q.: Chalcone Derivatives: Role in Anticancer Therapy. Biomolecules. 11, 894 (2021). https://doi.org/10.3390/biom11060894

2. Heba, P.: Chemical and Structural Properties of Chalcones I.

3. Herencia, F., Ferrándiz, M.L., Ubeda, A., Domínguez, J.N., Charris, J.E., Lobo, G.M., Alcaraz, M.J.: Synthesis and anti-inflammatory activity of chalcone derivatives. Bioorg Med Chem Lett. 8, 1169–1174 (1998). https://doi.org/10.1016/s0960-894x(98)00179-6

4. Huzinaga, S., Sakai, Y., Miyoshi, E., Narita, S.: Extended Mulliken electron population analysis. J. Chem. Phys. 93, 3319–3325 (1990). https://doi.org/10.1063/1.458812

5. Priya, M.K., Revathi, B.K., Renuka, V., Sathya, S., Asirvatham, P.S.: Molecular Structure, Spectroscopic (FT-IR, FT-Raman, 13C and 1H NMR) Analysis, HOMO-LUMO Energies, Mulliken, MEP and Thermal Properties of New Chalcone Derivative by DFT Calculation. Materials Today: Proceedings. 8, 37–46 (2019). https://doi.org/10.1016/j.matpr.2019.02.078

6. Anbarasan, R., Kalyana Sundar, J.: Experimental and quantum chemical investigation on imidazolium trifluoroacetate single crystal for optoelectronic applications. J Mater Sci: Mater Electron. 30, 10224–10232 (2019). https://doi.org/10.1007/s10854-019-01359-0

7. Khajehzadeh, M., Sadeghi, N.: Molecular structure, the effect of solvent on UV–vis and NMR, FT–IR and FT–Raman spectra, NBO, frontier molecular orbital analysis of Mitomycin anticancer drug. Journal of Molecular Liquids. 256, 238–246 (2018). https://doi.org/10.1016/j.molliq.2018.01.099

8. Manchanayakage, R.: Designing and Incorporating Green Chemistry Courses at a Liberal Arts College To Increase Students' Awareness and Interdisciplinary Collaborative Work. J. Chem. Educ. 90, 1167–1171 (2013). https://doi.org/10.1021/ed300468r

9. Ismiyarto, I., Matsjeh, S., Anwar, C.: Synthesis of Chalcone and Flavanone Compound Using Raw Material of Acetophenone and Benzaldehyde Derivative. Indonesian Journal of Chemistry. 1, 81–89 (2010). https://doi.org/10.22146/ijc.21948

10. Liao, T., Ye, W., Chen, D., Qin, Y., Chen, Y., Liao, W., Zhou, Z.: Synthesis, crystal structure, and DFT study of 4-(2-Chlorobenzyl)-1-(furan-2-yl)-[1,2,4]triazolo[4,3-a]quinazolin-5(4H)-one. Journal of Heterocyclic Chemistry. 59, 137–143 (2022). https://doi.org/10.1002/jhet.4373

11. Sheldrick, G.: shelxs97 and shelxl97. University of Göttingen, Germany. 4, (1997)

12. Sheldrick, G.M.: Crystal structure refinement with SHELXL. Acta Cryst C. 71, 3–8 (2015). https://doi.org/10.1107/S2053229614024218

13. Naik, V.S., Patil, P.S., Wong, Q.A., Quah, C.K., Gummagol, N.B., Jayanna, H.S.: Molecular structure, linear optical, second and third-order nonlinear optical properties of two non-centrosymmetric thiophene-chalcone derivatives. Journal of Molecular Structure. 1222, 128901 (2020). https://doi.org/10.1016/j.molstruc.2020.128901

14. Spek, A.L.: Single-crystal structure validation with the program PLATON. J Appl Cryst. 36, 7–13 (2003). https://doi.org/10.1107/S0021889802022112

15. Abosalim, H.M., Nael, M.A., El-Moselhy, T.F.: Design, Synthesis and Molecular Docking of Chalcone Derivatives as Potential Anticancer Agents. ChemistrySelect. 6, 888–895 (2021). https://doi.org/10.1002/slct.202004088

16. Qin, H.-L., Shang, Z.-P., Jantan, I., Tan, O.U., Hussain, M.A., Sher, M., Bukhari, S.N.A.: Molecular docking studies and biological evaluation of chalcone based pyrazolines as tyrosinase inhibitors and potential anticancer agents. RSC Adv. 5, 46330–46338 (2015). https://doi.org/10.1039/C5RA02995C

17. San-Martin, A., Donoso, V., Leiva, S., Bacho, M., Nunez, S., Gutierrez, M., Rovirosa, J., Bailon-Moscoso, N., Camacho, S.C., Aviles, O.M., Cazar, M.-E.: Molecular Docking Studies of the Antitumoral Activity and Characterization of New Chalcone. Curr Top Med Chem. 15, 1743–1749 (2015). https://doi.org/10.2174/1568026615666150427125033

18. Tyagi, N., Yadav, H., Hussain, A., Kumar, B.: Development of new L- Serine Squarate single crystal: Growth, structure, Hirshfeld surface analysis with enrichment ratio of atomic contacts. Journal of Molecular Structure. 1224, 129190 (2021). https://doi.org/10.1016/j.molstruc.2020.129190

19. Tan, S.L., Azizan, A.H.S., Jotani, M.M., Tiekink, E.R.T.: 3,3-Bis(2-hy-droxy-eth-yl)-1-(4-methyl-benzoyl)thio-urea: crystal structure, Hirshfeld surface analysis and computational study. Acta Crystallogr E Crystallogr Commun. 75, 1472–1478 (2019). https://doi.org/10.1107/S2056989019012581

20. Aksöz, B.E., Ertan, R.: Chemical and Structural Properties of Chalcones I. 20 (2011)

21. Tan, S.L., Jotani, M.M., Tiekink, E.R.T.: Utilizing Hirshfeld surface calculations, non-covalent inter-action (NCI) plots and the calculation of inter-action energies in the analysis of mol-ecular packing. Acta Crystallogr E Crystallogr Commun. 75, 308–318 (2019). https://doi.org/10.1107/S2056989019001129

22. Pinto, C.B., Dos Santos, L.H.R., Rodrigues, B.L.: Understanding metal–ligand inter-actions in coordination polymers using Hirshfeld surface analysis. Acta Cryst C. 75, 707–716 (2019). https://doi.org/10.1107/S2053229619005874

23. Seth, S.K.: Structural characterization and Hirshfeld surface analysis of a CoII complex with imidazo[1,2-a]pyridine. Acta Cryst E. 74, 600–606 (2018). https://doi.org/10.1107/S2056989018003857

24. Ferjani, H.: Structural, Hirshfeld Surface Analysis, Morphological Approach, and Spectroscopic Study of New Hybrid Iodobismuthate Containing Tetranuclear 0D Cluster Bi4I16·4(C6H9N2) 2(H2O). Crystals. 10, 397 (2020). https://doi.org/10.3390/cryst10050397

25. Kamath, L., Menezes, A.P., Bairy, R., Kumara swamy, S.K., Jayarama, A.: Hirshfeld surface analysis, enrichment ratio, energy frameworks and third-order nonlinear optical studies of a hydrazone derivative for optical limiting applications. Journal of Molecular Structure. 1245, 131019 (2021). https://doi.org/10.1016/j.molstruc.2021.131019

26. McKinnon, J.J., Spackman, M.A., Mitchell, A.S.: Novel tools for visualizing and exploring intermol-ecular interactions in molecular crystals. Acta Cryst B. 60, 627–668 (2004). https://doi.org/10.1107/S0108768104020300

27. Mackenzie, C.F., Spackman, P.R., Jayatilaka, D., Spackman, M.A.: CrystalExplorer model energies and energy frameworks: extension to metal coordination compounds, organic salts, solvates and open-shell systems. IUCrJ. 4, 575–587 (2017). https://doi.org/10.1107/S205225251700848X

28. Morris, G.M., Lim-Wilby, M.: Molecular Docking. In: Kukol, A. (ed.) Molecular Modeling of Proteins. pp. 365–382. Humana Press, Totowa, NJ (2008)

29. Wang, G., Zhu, W.: Molecular docking for drug discovery and development: a widely used approach but far from perfect. Future Medicinal Chemistry. 8, 1707–1710 (2016). https://doi.org/10.4155/fmc-2016-0143

30. Arjun, H.A., Rajan, R.K., Elancheran, R., Ramanathan, M., Bhattacharjee, A., Kabilan, S.: Crystal structure, Hirshfeld surface analysis, DFT and molecular docking studies on benzohydrazide derivatives as potential inhibitors of prostate cancer. Chemical Data Collections. 26, 100350 (2020). https://doi.org/10.1016/j.cdc.2020.100350

31. Patel, U.H., Gandhi, S.A., Barot, V.M., Patel, M.C.: A comparative study of novel chalcone derivative by X-ray and quantum chemical calculations (Ab-initio and DFT): Experimental and theoretical approach. Molecular Crystals and Liquid Crystals. 624, 190–204 (2016). https://doi.org/10.1080/15421406.2015.1011494

32. Kaya, S., Gökce, H., Arslan, T., Alpaslan, G.: Synthesis, spectroscopic characterization, DFT computations, nonlinear optical profile and molecular docking study of a novel chalcone derivative. Journal of Molecular Structure. 1202, 127270 (2020). https://doi.org/10.1016/j.molstruc.2019.127270

33. Aksöz, B.E., Ertan, R.: Chemical and Structural Properties of Chalcones I. 20 (2011)

34. Costa, J.C.S., Taveira, R.J.S., Lima, C.F.R.A.C., Mendes, A., Santos, L.M.N.B.F.: Optical band gaps of organic semiconductor materials. Optical Materials. 58, 51–60 (2016). https://doi.org/10.1016/j.optmat.2016.03.041

35. Xue, Y., Mou, J., Liu, Y., Gong, X., Yang, Y., An, L.: An ab initio simulation of the UV/Visible spectra of substituted chalcones. Open Chemistry. 8, 928–936 (2010). https://doi.org/10.2478/s11532-010-0058-3

36. Rajesh Kumar, P.C., Ravindrachary, V., Janardhana, K., Poojary, B.: Structural and optical properties of a new chalcone single crystal. Journal of Crystal Growth. 354, 182–187 (2012). https://doi.org/10.1016/j.jcrysgro.2012.06.006

37. Muhammad, S., Al-Sehemi, A.G., Irfan, A., Algarni, H., Qiu, Y., Xu, H., Su, Z., Iqbal, J.: The substitution effect of heterocyclic rings to tune the optical and nonlinear optical properties of hybrid chalcones: A comparative study. Journal of Molecular Graphics and Modelling. 81, 25–31 (2018). https://doi.org/10.1016/j.jmgm.2018.02.005

Tables

Table 1: Crystal Parameters

CCDC Deposition	2151070
Molecular formula	C_{15} H_9 Cl F_2 O
Formula weight	278.67
Space Group	P -1
Cell length ‘a’	3.9614(4)Å
Cell length ‘b	6.0101(6)Å
Cell length ‘c	26.069(2)Å
Interfacial angle ‘α’	92.452(6)˚
Interfacial angle ‘β’	91.025(6)˚
Interfacial angle ‘γ’	92.483(7)˚
Cell volume	619.39(10)Å^3
Z	2
Density = ρ	1.494 calc./mg mm^{-3}
Structure factor evaluated in the zeroth-order case = F_{000}	284
Theta range for data collection	0.78º to 25.24º
Index ranges	$-5 \leq h \leq 5, -6 \leq k \leq 7, -33 \leq l \leq 33$
Reflections collected	9284
Number of unique reflections	2755
Number of intense reflections	1616
R	0.0529
Goodness of fit S on F^2	0.977
Absorption coefficient	0.320 μ/mm^{-1}

Largest diff. peak and hole	0.175 and -0.250(0.046)e.$Å^{-3}$

Table 2: Hirshfeld Surface data

HS	Range	Mean
Shape index	-1.0 to 1.0 (-0.9925 to 0.9989)	0.2757
Curvdness	-4.0 to 4.0 (-4.4943 to 0.2389)	0.2757
Fragment patch	0 to 13 mean	6.9187
Volume	303.54 $Å^3$	
Area	0.749$Å^2$	
Globularity	0.429	

Table 3: 2D Fingerprint data

	% OF CONTRIBUTION				
EXT↓ INT→	CL	F	O	C	H
CL	2	0	0	0	13.7
F	0	1.4	0.5	4.5	17.7
O	0	0.5	0.1	0.2	9.5
C	0	4.5	0.2	14.4	9.8
H	13.7	17.7	9.5	9.8	24.5

Table 4: Internal Energy data

Energy Model	k_ele	k_pol	k_disp	k_rep
CE-HF ... HF/3-21G electron densities	1.019	0.651	0.901	0.811
CE-B3LYP ... B3LYP/6-31G(d,p) electron densities	1.057	0.740	0.871	0.618

Table 5: Interaction Energies (kJ/mol)

	N	Symop	R	Electron Density	E_ele	E_pol	E_dis	E_rep	E_tot
	1	-x, -y, -z	16.43	B3LYP/6-31G(d,p)	-4.8	-0.0	-3.3	0.0	-8.0
	2	x, y, z	7.05	B3LYP/6-31G(d,p)	-7.2	-2.3	-20.9	13.9	-19.0
	2	x, y, z	3.96	B3LYP/6-31G(d,p)	-3.1	-0.6	-66.2	32.0	-41.7
	1	-x, -y, -z	14.48	B3LYP/6-31G(d,p)	-5.0	-0.3	-7.1	0.0	-11.7
	1	-x, -y, -z	13.26	B3LYP/6-31G(d,p)	-9.2	-0.5	-8.3	0.0	-17.3
	2	x, y, z	6.01	B3LYP/6-31G(d,p)	-6.1	-2.1	-29.2	15.1	-24.2
	1	-x, -y, -z	13.41	B3LYP/6-31G(d,p)	-2.9	-0.5	-9.4	0.0	-11.5
	1	-x, -y, -z	14.03	B3LYP/6-31G(d,p)	3.0	-0.1	-6.8	0.0	-2.7
	1	-x, -y, -z	15.22	B3LYP/6-31G(d,p)	-7.6	-0.3	-6.9	0.0	-14.2

Table 6: The dock results of the ligand (lak) with 1KZN

Compound	Binding Energy (kJ mol^{-1})	Ligand Efficiency	Inhibition Constant	vdW+ H-bond + desolv energy	No. of H-bonds	Bonding residues	Bond Length(Å)
$C_{15}H_9ClF_2O$	-6.99	-0.3	7.47	-9.13	1	1KZN: A: GLY77: HN	1.88

Table 7: Calculated electronic excitations and spectral details.

Functional	Excited State	Excitation Energy	Wavelength λ(nm)	Oscillatory strength (f)	Major Contribution
B3LYP	1	3.1251 eV	396.74 nm	f = 0.0000	(HOMO) 73 -> 76 (LUMO)-69.49%
	2	3.6396 eV	340.65 nm	f = 0.5549	(HOMO) 75 -> 76 (LUMO)-69.94%

	3	4.0525 eV	305.94 nm	f = 0.2065	(HOMO) 74 -> 76 LUMO)-62.30%
					(HOMO) 75 -> 77 (LUMO)-11.17%
					(HOMO) 72 -> 76 (LUMO)--28.68%

Table 8: Calculated Homo-Lumo, Energy gap and other molecular properties.

HOMO E_{HOMO}	-6.43 eV
LUMO E_{LUMO}	-2.43 eV
Energy Gap E_g	4.0 eV
Ionization potential ($I=-E_{HOMO}$)	6.40 eV
Electron Affinity ($A=-E_{LUMO}$)	2.43 eV
Chemical Potential ($\mu = -(I+A)/2$)	-4.42 eV
Hardness ($\eta =(I-A)/2$)	1.98 eV
Softness ($S =1/2\eta$)	0.25 eV
Electronegativity ($\chi = (I+A)/2$)	4.42 eV
Electrophilicity index ($\omega = \mu^2/2\eta$)	4.93 eV

Table 9: XRD data-Bond length between atoms of the molecule from experiment and theory

Atoms		**Bod length**	
		Experiment	DFT
Cl1	C2	1.733(3)	1.733
F18	C17	1.352(3)	1.352
F19	C15	1.349(3)	1.349
O11	C10	1.220(4)	1.220

C2	C3	1.365(4)	1.365
C2	C7	1.385(4)	1.385
C3	C4	1.373(4)	1.373
C4	C5	1.399(4)	1.399
C5	C6	1.387(4)	1.387
C5	C8	1.453(4)	1.453
C6	C7	1.371(4)	1.371
C8	C9	1.316(4)	1.316
C9	C10	1.470(4)	1.470
C10	C12	1.499(4)	1.499
C12	C13	1.397(4)	1.397
C12	C17	1.386(4)	1.386
C13	C14	1.371(4)	1.371
C14	C15	1.366(5)	1.366
C15	C16	1.353(5)	1.353
C16	C17	1.374(4)	1.374
C3	H3	0.93	1.083
C4	H4	0.93	1.083
C6	H6	0.93	1.083
C7	H7	0.93	1.083
C8	H8	0.93	1.083
C9	H9	0.93	1.083
C13	H13	0.93	1.083
C14	H14	0.93	1.083
C16	H16	0.93	1.083

Table 10: XRD-Bond angle between atoms of the molecule

Atoms	Geometrical bond angle
Cl1 C2 C3	120.0(2)
Cl1 C2 C7	119.3(2)

C3 C2 C7	120.7(3)
C2 C3 C4	119.4(2)
C3 C4 C5	121.4(3)
C4 C5 C6	117.7(2)
C4 C5 C8	119.2(3)
C6 C5 C8	123.0(2)
C5 C6 C7	121.0(2)
C2 C7 C6	119.7(3)
C5 C8 C9	128.4(3)
C8 C9 C10	120.3(3)
O11 C10 C9	121.0(2)
O11 C10 C12	117.6(3)
C9 C10 C12	121.4(3)
C10 C12 C13	117.4(3)
C10 C12 C17	127.3(3)
C13 C12 C17	115.3(2)
C12 C13 C14	122.5(3)
C13 C14 C15	118.5(3)
F19 C15 C14	119.2(3)
F19 C15 C16	118.4(3)
C14 C15 C16	122.4(3)
C15 C16 C17	117.9(3)
F18 C17 C12	120.3(2)
F18 C17 C16	116.1(3)
C12 C17 C16	123.5(3)
C2 C3 H3	120
C4 C3 H3	120
C3 C4 H4	119
C5 C4 H4	119
C5 C6 H6	120
C7 C6 H6	119
C2 C7 H7	120

C6 C7 H7	120
C5 C8 H8	116
C9 C8 H8	116
C8 C9 9	120
C10 C9 H9	120
C12 C13 H13	119
C14 C13 H13	119
C13 C14 H14	121
C15 C14 H14	121
C15 C16 H16	121
C17 C16 H16	121

FIGURE CAPTIONS

Figure 1:The structure of Chalcone.

Figure 2: ORTEP diagram of the title compound.

Figure 3: Packing diagram of the title molecule. Dotted line indicates the hydrogen bond.

Figure 4: Hirshfeld surface (d_{norm}).

Figure 5: Hirshfeld surface (d_{norm}) with close intermolecular contacts with bond lengths.

Figure 6. (a) π - π stacking interactions (Shape index)(b) π - π stacking interactions (Shape index).

Figure 7: Hirshfeld surface (curvedness).

Figure 8: Hirshfeld surface (fragment patch).

Figure 9 (a-j): Hirshfeld surface with 2D fingerprint plot.

Figure 10: The building of energy frameworks.

Figure 11: Hydrogen bond interaction at the active site amino acid residue Gly77 at a distance of 1.88 Å.

Figure 12: Ligand Receptor Complex.

Figure 13: Optimised structure of the molecule.

Figure 14 (a). UV-visible spectra of C15H9ClF2O molecule. (b).Tauc's Plot of C15H9ClF2O molecule.

Figure 15: IR spectrum of $C_{15}H_9ClF_2O$ molecule.

Figure 16: Molecular electrostatic potential map.

Figure 17: Molecular orbitals (HOMO–LUMO).

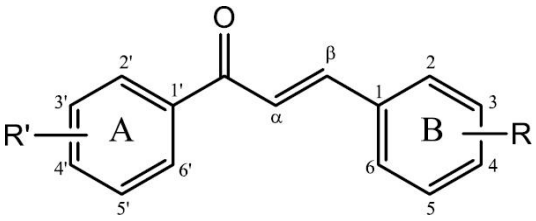

Fig. 1.

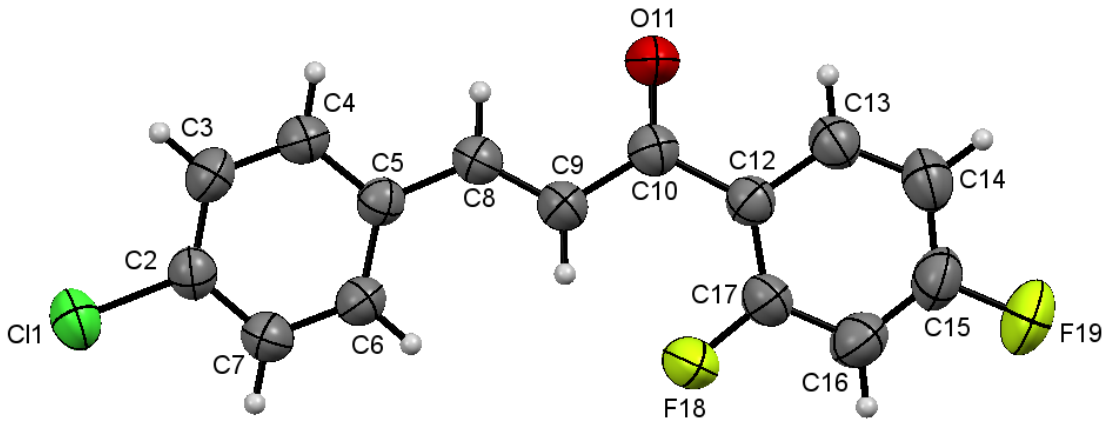

Fig. 2.

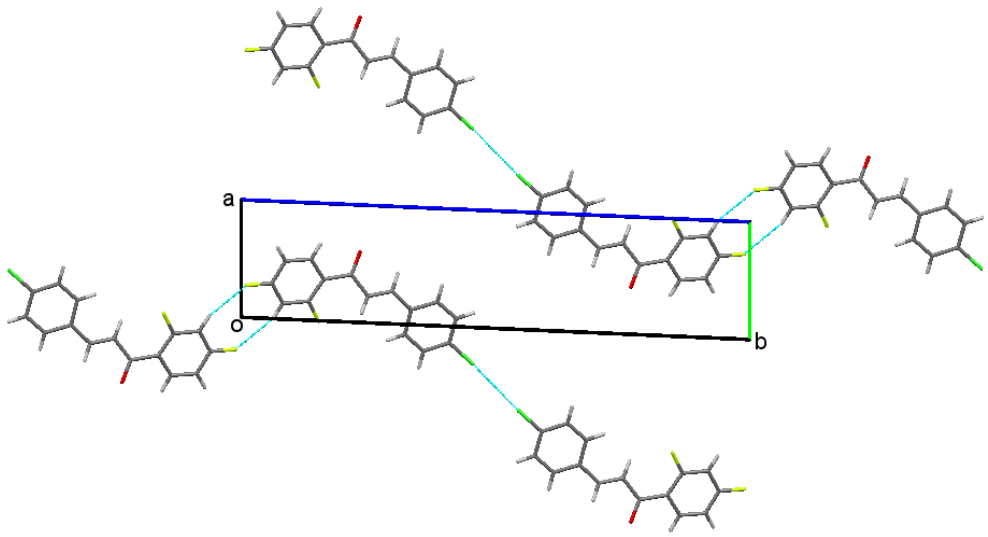

Fig. 3.

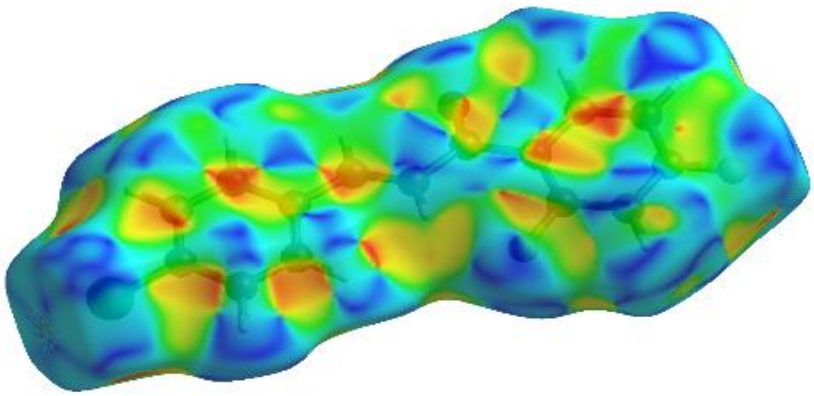

Fig. 4.

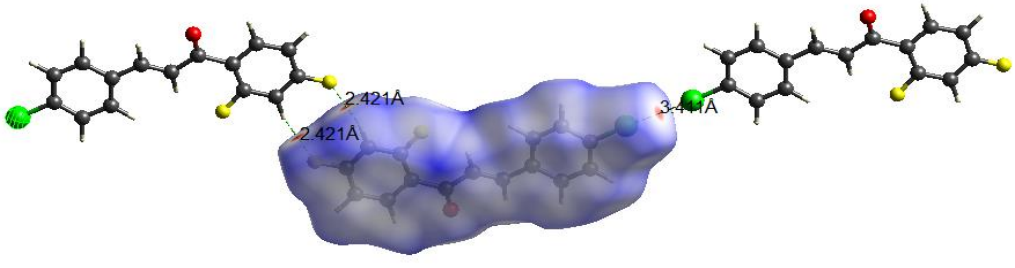

Fig. 5.

(a) (b)

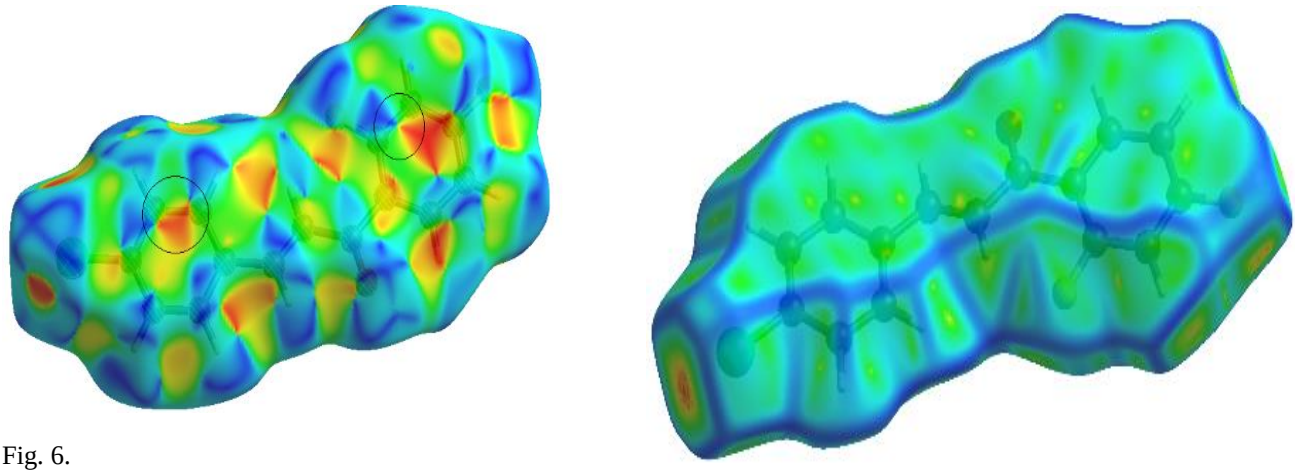

Fig. 6.

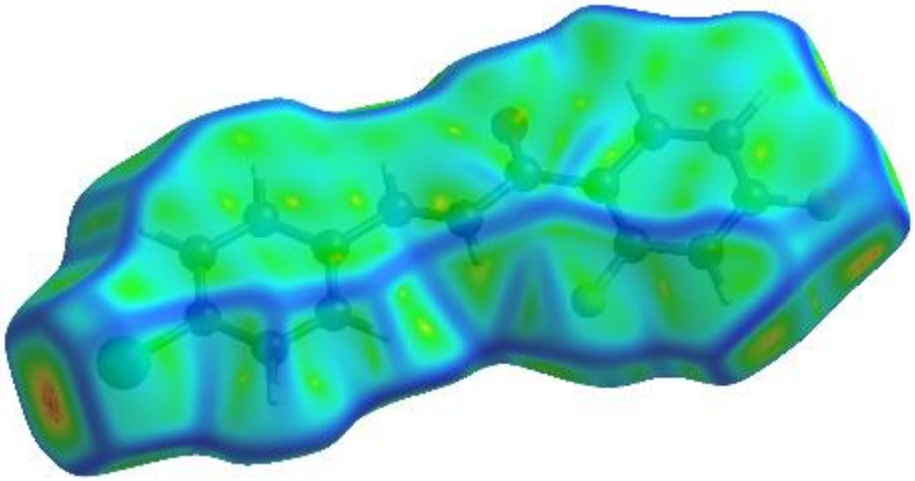

Fig. 7.

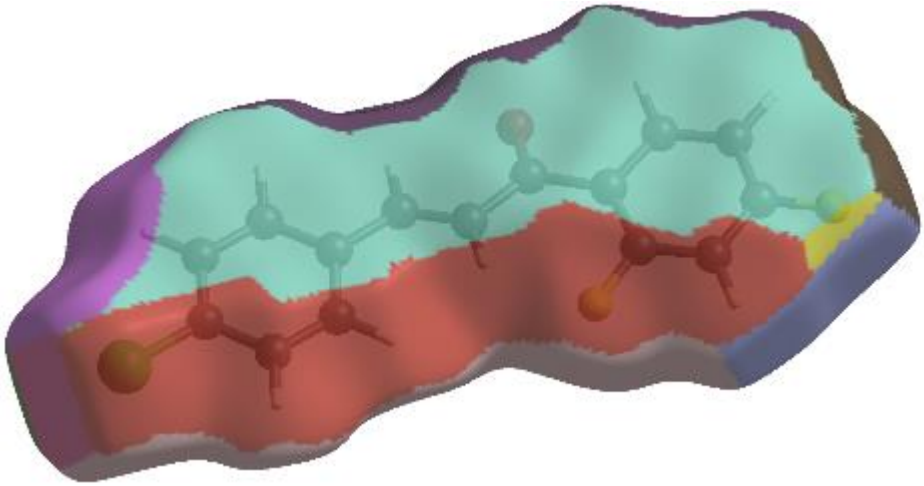

Fig. 8.

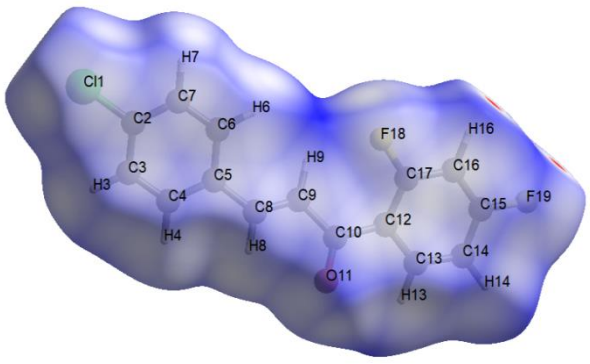

Figure 9 (a): OVERALL PACKING

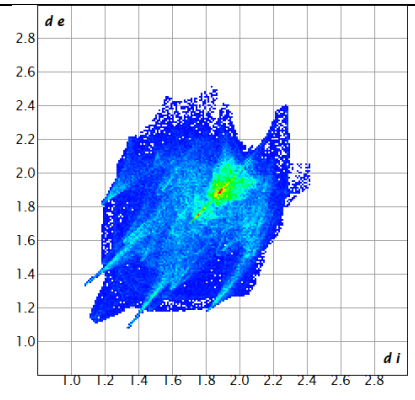

OVERALL PACKING-100%

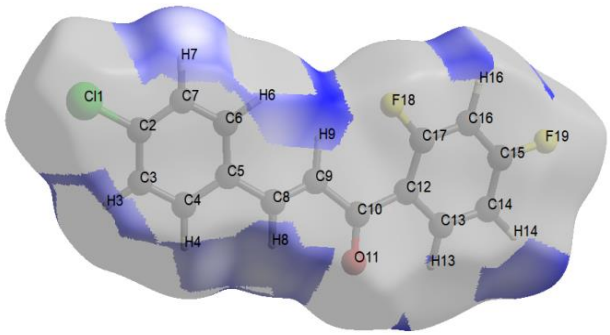

Figure 9(b): H…H - HS

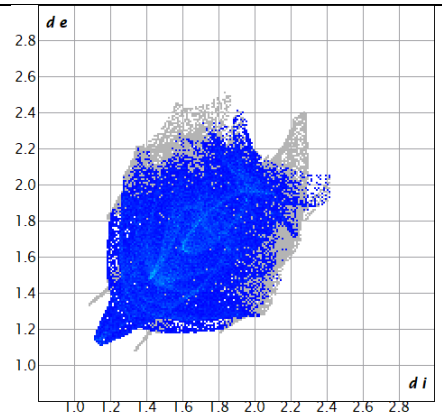

H…H – 24.5%

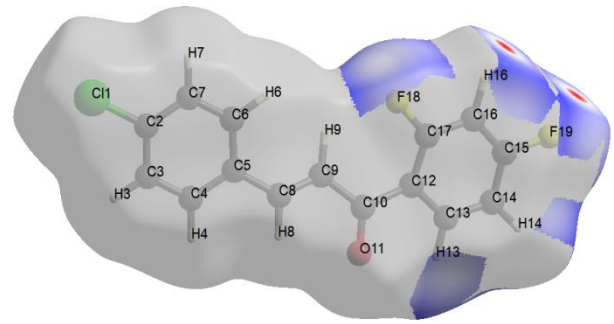

Figure 9(d): C…C – HS

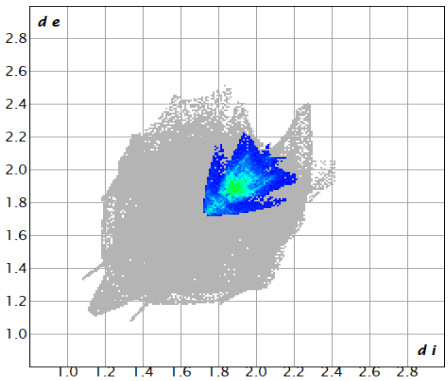

C…C – 14.4%

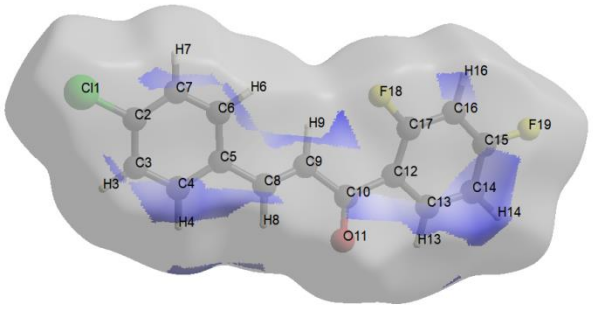

Figure 9(e): C…H/H…C - HS

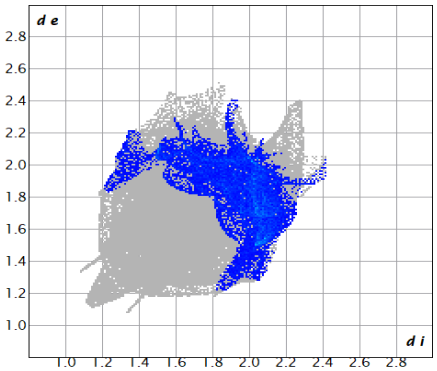

C…H/H…C – 9.8%

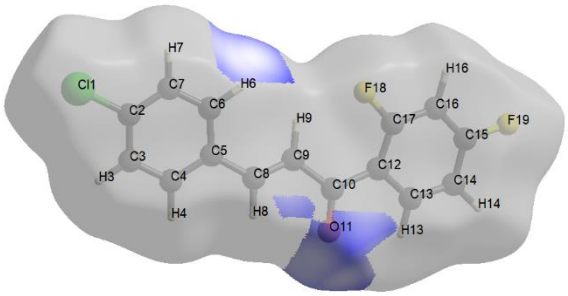

Figure 9(f): O…H/H…O-HS

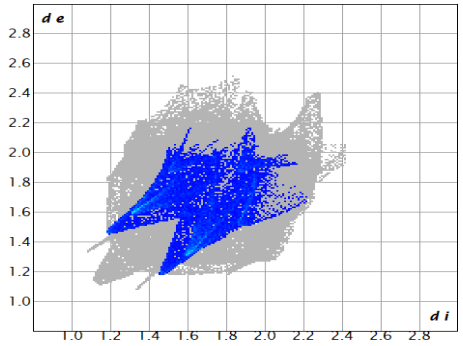

O…H/H…O – 9.5%

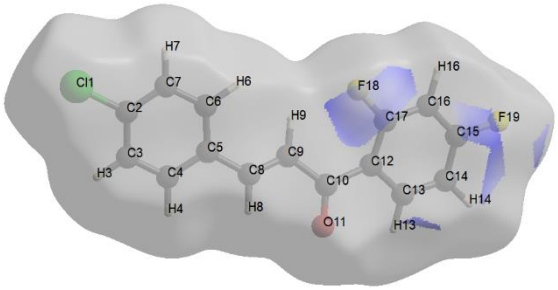

Figure 9(g): F…C/C…F-HS

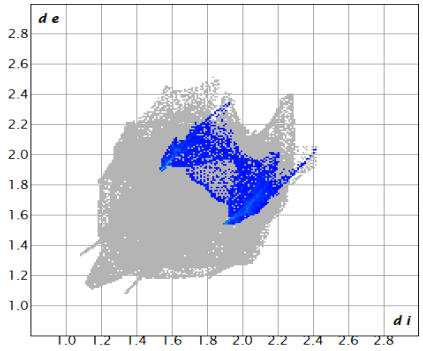

F…C/C…F – 4.5%

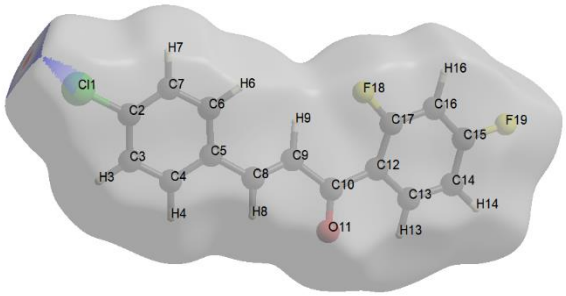

Figure 9(h): CL…CL - HS

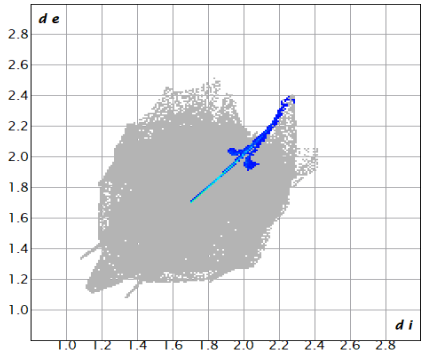

CL…CL – 2%

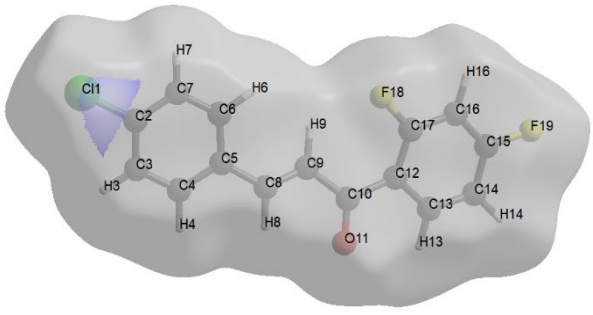

Figure 9(i): C…CL/CL…C - HS

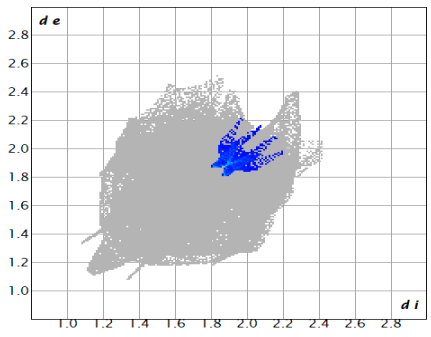

C…CL/CL…C – 1.7%

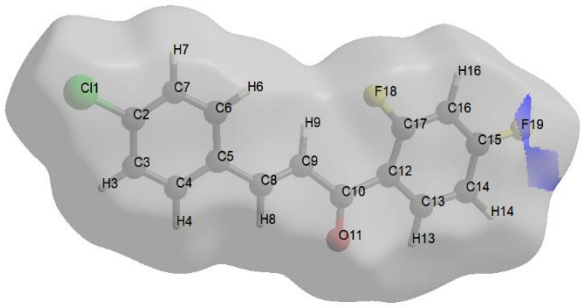

Figure 9(j): F…F/F…F - HS

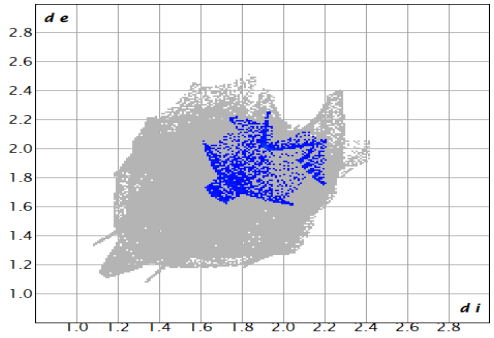

F…F/F…F - HS

Fig. 9.

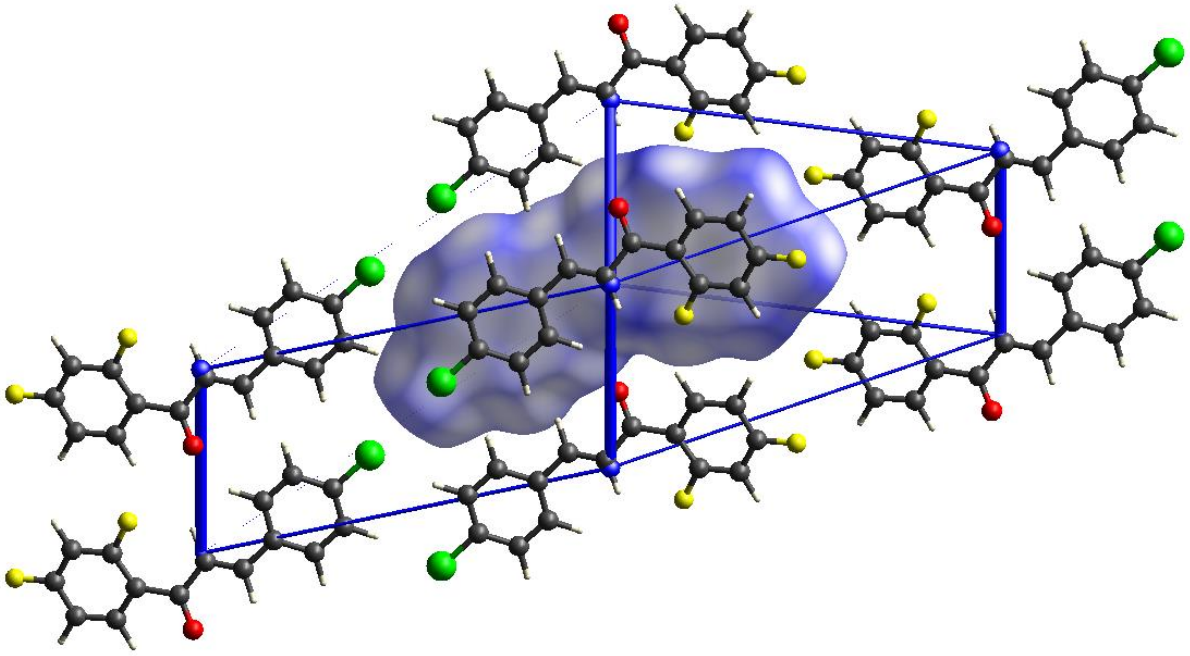

Fig. 10.

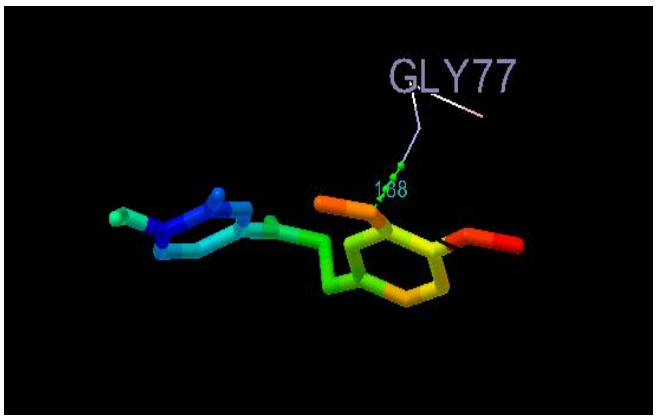

Fig. 11.

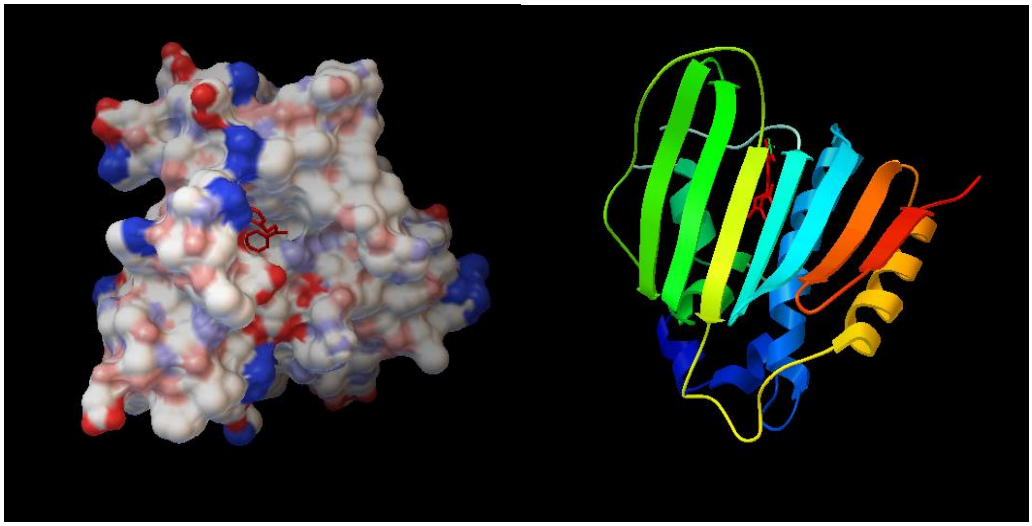

Fig. 12.

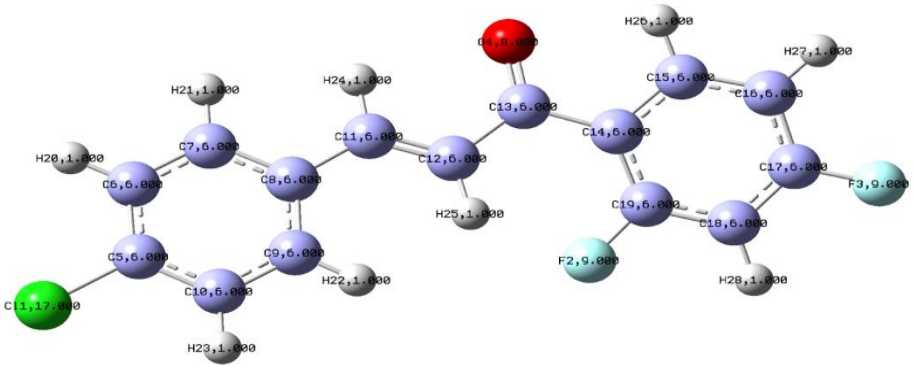
H26,1.000
O4,8.000
H27,1.000
C15,6.000
C16,6.000
H21,1.000
H24,1.000
C13,6.000
C14,6.000
C7,6.000
C11,6.000
H20,1.000
C12,6.000
C17,6.000
F3,9.000
C6,6.000
C8,6.000
H25,1.000
C19,6.000
C18,6.000
C5,6.000
C9,6.000
F2,9.000
H22,1.000
H28,1.000
C10,6.000
Cl1,17.000
H23,1.000

Fig. 13.

(a)

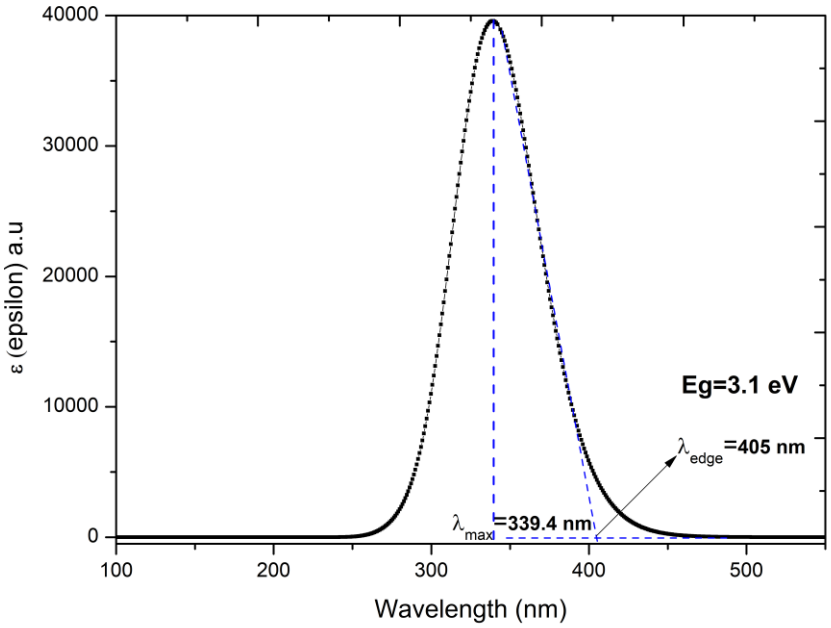
40000
30000
20000
10000
0
ε (epsilon) a.u
100
200
300
400
500
Wavelength (nm)
Eg=3.1 eV
λedge=405 nm
λmax=339.4 nm

(b)

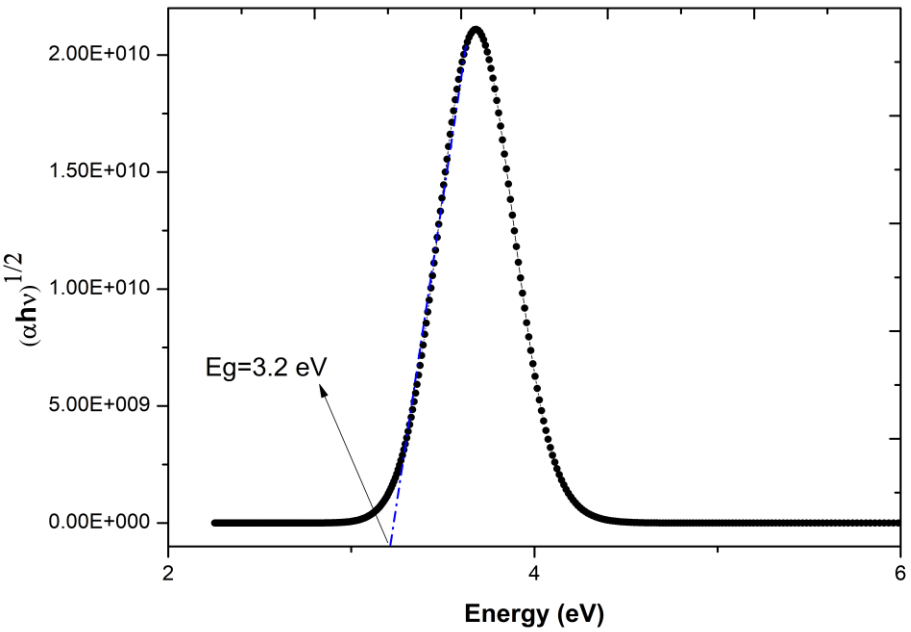
2.00E+010
1.50E+010
1.00E+010
5.00E+009
0.00E+000
(αhν)1/2
2
4
6
Energy (eV)
Eg=3.2 eV

Fig. 14

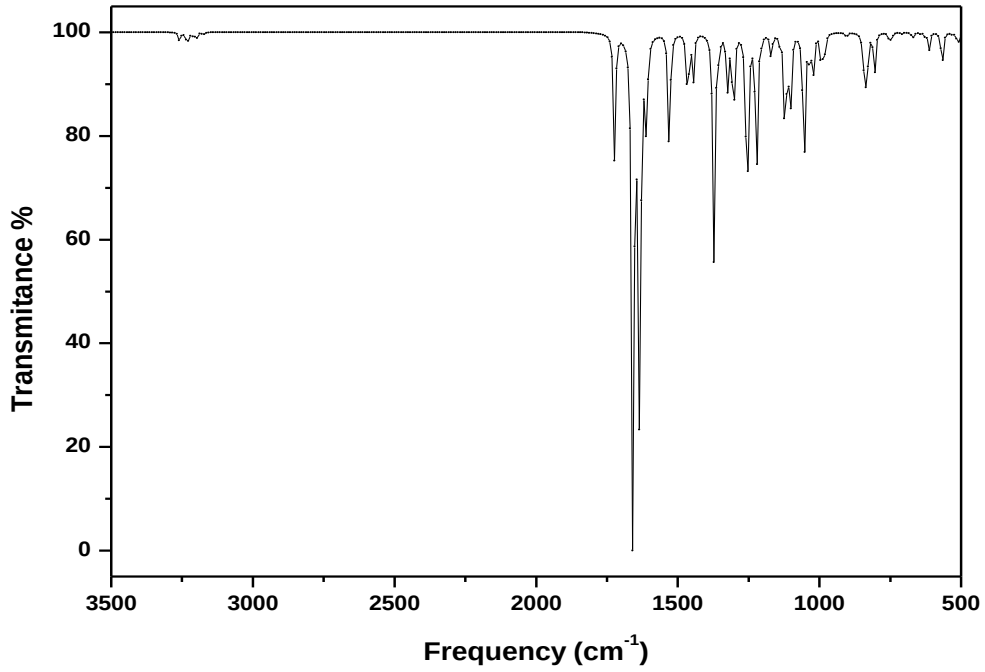
Transmitance %
100
80
60
40
20
0
3500
3000
2500
2000
1500
1000
500
Frequency (cm-1)

Fig. 15.

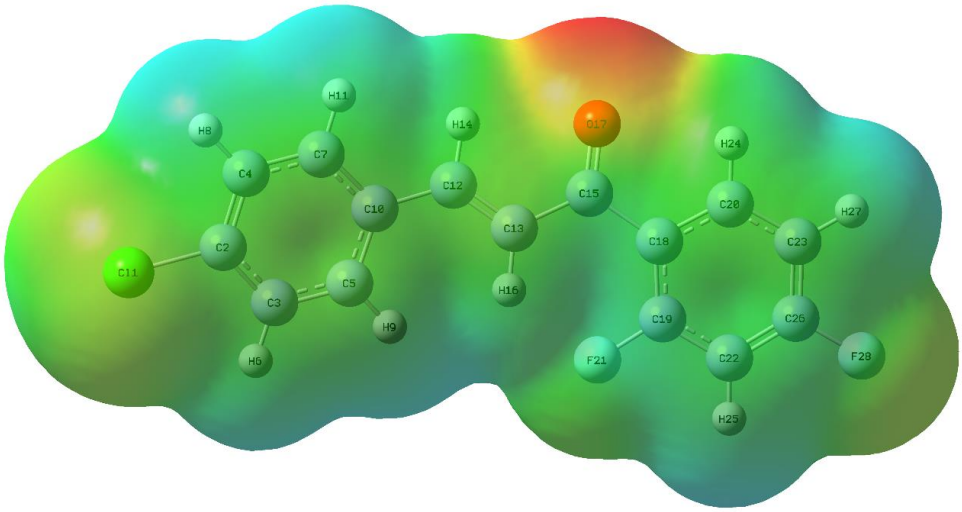
H11
H8
C7
C4
H14
C12
C10
C15
O17
H24
C20
H27
C23
C2
C11
C5
C3
C13
C18
H16
H9
H6
C19
C26
F21
C22
F23
H25

Fig. 16.

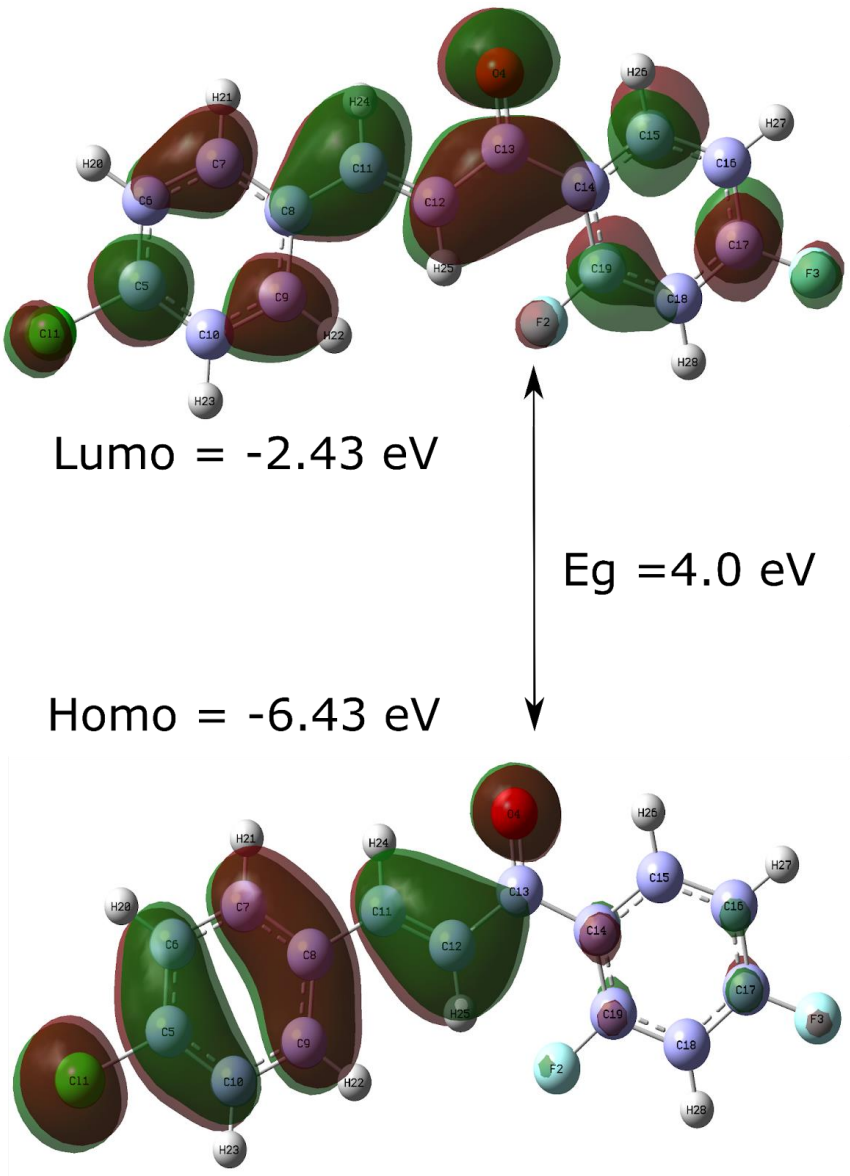

Fig. 17.